research papers

A novel comparative study of crystalline perfection and optical homogeneity in Nd:GGG crystals grown by the Czochralski technique with different crystal/melt interface shapes

Khavangkhui Zimik,[a] G. Bhagavannarayana,[b]* Ramesh Kumar,[a] Rashmi Rai Chauhan,[a] Krishna Murari,[a] Neelam Malhan[a] and Harneet V. Thakur[c]

[a]Laser Science and Technology Centre, Defence Research and Development Organization, Delhi 110 054, India, [b]CSIR–National Physical Laboratory, Dr K. S. Krishnan Road, New Delhi 110 012, India, and [c]Armament Research and Development Establishment, Pune 411 021, India. Correspondence e-mail: bhagavan@nplindia.org

Nd:GGG crystals (GGG is gadolinium gallium garnet) grown with different crystal/melt interface shapes (convex/flat/concave) by varying the seed rotation rate while using the Czochralski technique were studied for their optical homogeneity and crystalline perfection by optical polarization microscopy (OPM) and high-resolution X-ray diffractometry (HRXRD), respectively. It was found that there is a remarkable effect of seed rotation rate, which decides the shape of the crystal/melt interface, on the optical homogeneity and crystalline perfection. It was found experimentally that, as the rotation rate increases, the crystal/melt interface changes from convex to flat. If the rate further increases the interface becomes concave. With a steep convex interface (for low rotation rates), certain facets are concentrated in the small central portion of the crystal, and as the rate increases, these facets slowly move outward, leading to improved optical homogeneity and crystalline perfection as observed from the OPM and HRXRD results. The strain developed in the crystalline matrix as a result of segregation of oxygen in the crystals at low seed rotation rates as observed from HRXRD seems to be the reason for the observed optical inhomogeneity. The correlation between optical inhomogeneity and crystalline perfection for a variety of specimens with different shapes of the crystal/liquid interface obtained at different seed rotation rates is reported.

1. Introduction

The gadolinium gallium garnet (GGG, $Gd_3Ga_5O_{12}$) crystal belongs to the rare earth garnets, which are generally considered cubic and have space group $Ia3d$, with Gd^{3+} located in dodecahedral c sites, and Ga^{3+} in octahedral a sites and tetrahedral d sites (Lupei *et al.*, 1997; Keszei *et al.*, 2001). GGG is generally grown by the Czochralski crystal growth technique. It is used in the fabrication of various optical components and as a substrate material for magneto-optical films such as gadolinium iron garnet with suitable dopants like Mg, Zr and Cr, and is as an excellent material for magneto-optic memory/display devices (Greber, 2002). The other important property of GGG is that it acts as a good lasing medium for solid-state lasers. In Nd:GGG lasers, the dopant, triply ionized neodymium, Nd^{III} (Nd^{3+}), typically replaces a small fraction of the gadolinium ions, Gd^{3+}, in the host crystal structure. However, there is one inherent problem in the growth of GGG/Nd:GGG crystals by the Czochralski technique, which is the formation of growth facets. An Nd:GGG crystal grown along ⟨111⟩ contains two distinct areas of facet

formation: a central area or core composed of three (211) facets and a middle area composed of three additional (110) facets, as shown in Fig. 1(*a*). At low crystal rotation rates, the crystal/melt interface is convex. Facet formation and resulting
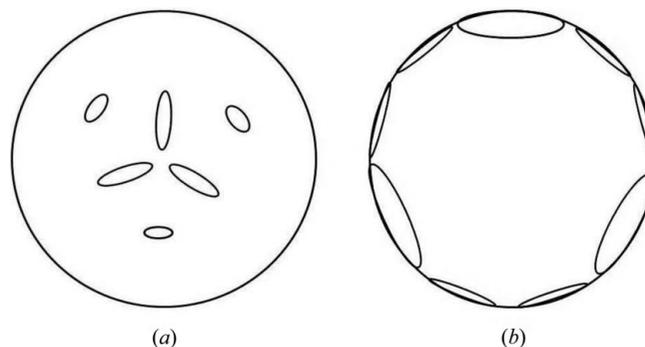
Figure 1
Facet positioning of a ⟨111⟩-grown garnet crystal at (*a*) a slow crystal rotation rate (convex interface) and (*b*) a fast crystal rotation rate (flat interface).

strain usually occur in the crystal/melt interface whenever the curvature of the solid/liquid interface passes through one of these directions and becomes tangent to the direction of naturally occurring facets (Janusz *et al.*, 1982). The similarities in the strain level between facet and matrix in both yttrium aluminium garnet and GGG suggest that the same mechanism operates in both materials, and the common element in these two materials is oxygen. Therefore the oxygen segregation effect, *i.e.* oxygen vacancies found in the facet region, is the most likely mechanism (Janusz *et al.*, 1982) that leads to an inhomogeneous central core when the crystal/melt interface is convex. Stacy *et al.* (1974) have reported that the faceted/inhomogeneous central region of a GGG crystal contains more oxygen vacancies than the regions away from the faceted region.

The interface shape influences the quality of crystals grown by the Czochralski technique. With a steep convex interface, the facets are concentrated in the small central portion of the crystal. These facets produce macroscopic strain patterns which are normally displaced about the growth axis, and for this reason the whole crystal is unsuitable for use in device applications. As the rotation increases, the facets slowly move outward, and at fast rotation rates, when the interface becomes flat, the facets are pushed towards the rim of the crystal, as shown in Fig. 1(*b*). In this case, we can use most of the crystal. When the crystal rotation is further increased, this leads to concave growth and the inhomogeneous central core can be eliminated.

In the present investigation, the growth of Nd:GGG was carried out by the Czochralski technique with different crystal/melt interface shapes, *viz.* a steep convex interface (with facets), a flat interface (facet free) and a concave interface (facet free). The crystalline perfection of the above Nd:GGG single crystals was characterized by using a polarizing microscope and high-resolution X-ray diffraction by employing a multicrystal X-ray diffractometer developed at the National Physical Laboratory (NPL) (Lal & Bhagavannarayana, 1989).

2. Experimental

2.1. Material preparation

The feed material was prepared by taking the stoichiometric composition of Gd_2O_3 (5 *N*) and Ga_2O_3 (5 *N*) and 1% of Nd_2O_3 (4 *N*) (Alfa Aesar, USA). The oxides were preheated at about 873 K for about 5 h before weighing. The materials were thoroughly mixed and polycrystalline material was prepared by heating it at 1273, 1473 and 1573 K for about 6–7 h each. After each stage of firing, the material was thoroughly mixed to homogenize the compound.

2.2. Crystal growth

Crystal growth was carried out by using an automatic diameter control Czochralski crystal puller from Cyberstar SA, France (Model Oxy-Puller 20–04), and in the presence of argon with 1.2% oxygen as this gives the best result (Zimik *et al.*, 2013). The polycrystalline Nd:GGG feed material was

taken in an iridium crucible and, after melting (melting point ∼2003 K) of the initial feed material, more material was poured through the funnel arrangement so that the melt was allowed to fill up to around 5 mm below the rim of the crucible. The melt temperature was adjusted for seeding by slowly increasing the power and by observing the disappearance of small islands at the center of the molten surface. A GGG crystal with ⟨111⟩ orientation was used as seed crystal. All the Nd:GGG crystals were grown with a growth or pulling rate of 1.5 mm h^{-1}. The crystal/melt interface depth was manipulated by crystal rotation, and different crystal rotations were employed during each growth experiment to obtain different interface depths/shapes. Optically polished samples of crystals grown with different interface shapes as observed under a polarizing microscope are shown in Fig. 2. To restrict the formation of facets to the central portion, the growth of the crystal in Fig. 2(*a*) was carried out with a convex crystal/melt interface (*i.e.* at a slow rotation of up to 20 r min^{-1}). The crystal in Fig. 2(*b*) was grown with a flat crystal/melt interface. Details of the method to grow crystals with a flat interface for different crucible sizes are described elsewhere (Zimik *et al.*, 2013). To maintain flat interface growth, when the crystal cylinder starts to form, the crystal rotation rate needs to be lowered consistently from the initial condition for a flat interface until the completion of crystal growth by about 5 r min^{-1} (for a crystal cylinder length of 50 mm) to compensate for the lowering of the melt. If the crystal rotation rate is not lowered from the initial condition or the crystal rotation is above what is required for flat interface growth, the crystal/melt interface will slowly become concave. The crystal in Fig. 2(*c*) was obtained in one such experiment.
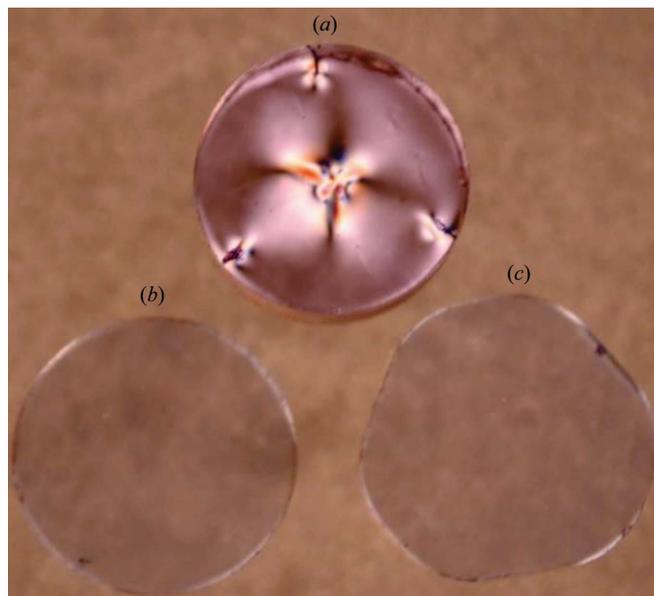
Figure 2
Cross-section views of Nd-doped GGG crystals as seen under polarized light; (*a*) an Nd:GGG crystal grown with a steep convex interface, (*b*) an Nd:GGG crystal grown with a flat interface and (*c*) an Nd:GGG crystal grown with a concave interface.

research papers

2.3. High-resolution X-ray diffraction

The above crystals grown with different interface shapes were analyzed for crystalline perfection using high-resolution X-ray diffraction (HRXRD) by employing a multicrystal X-ray diffractometer developed at NPL (Lal & Bhagavannarayana, 1989). The well collimated and monochromated Mo $K\alpha_1$ beam obtained from three monochromator Si crystals set in the dispersive $(+,-,-)$ configuration was used as the exploring X-ray beam. The specimen crystal was aligned in the $(+,-,-,+)$ configuration. As a result of using the dispersive configuration, though the lattice constant of the monochromator crystal(s) and the specimen are different, the unwanted dispersion broadening in the diffraction curve (DC) of the specimen crystal is insignificant. The specimen can be rotated about the vertical axis, which is perpendicular to the plane of diffraction, with a minimum angular interval of 0.4″. The rocking or diffraction curves were recorded by changing the glancing angle (the angle between the incident X-ray beam and the surface of the specimen) around the Bragg diffraction peak position θ_B (taken as zero for the sake of convenience), starting from a suitable arbitrary glancing angle and ending at a glancing angle after the peak so that all the meaningful scattered intensities on both sides of the peak are included in the diffraction curve. The DC was recorded by the so-called ω scan, wherein the detector was kept at the same angular position $2\theta_B$ with a wide opening for its slit. This arrangement is very appropriate for recording the short-range-order scattering caused by defects or by scattering from local Bragg diffraction from agglomerated point defects or by low-angle and very low angle structural grain boundaries (Bhagavannarayana & Kushwaha, 2010; SenthilKumar et al., 2011). It may be mentioned here that the ω scan is appropriate for obtaining information about defects only when the exploring beam or incident beam is highly monochromatic ($\Delta\lambda/\lambda \ll 10^{-5}$) and parallel ($\ll 3''$) and preferably low-wavelength radiation (Mo $K\alpha_1$) (Bhagavannarayana & Kushwaha, 2010), otherwise one has to use a triple-axis diffractometer with an analyzer crystal (Bhagavannarayana & Zaumseil, 1997). Even with such a system, details about very low angle boundaries could be missed.

Before the diffraction curve was recorded, in order to remove the noncrystallized solute atoms remaining on the surface of the crystal and the possible layers that sometimes form on the surfaces of crystals grown by solution methods (Bhagavannarayana et al., 2006), and to ensure surface planarity, the specimen was first lapped and chemically etched in a non-preferential etchant.

3. Results and discussion on HRXRD analyses

Fig. 3 shows the high-resolution DCs recorded from a clean (a) and the central region (b) of an Nd:GGG single crystal [specimen (a) of Fig. 2, which is also shown in the inset] grown with a steep convex interface. As seen in Fig. 3(a), the DC recorded from the clean region contains a single peak and indicates that the specimen is free from structural grain

boundaries. The full width at half-maximum (FWHM) of this curve is 18″, which shows that the crystalline perfection of this region is quite good. Fig. 3(b) is recorded from the central region, where there is a flower-type defective region. The FWHM is 30″, which is somewhat higher than that expected from the plane wave theory of dynamical X-ray diffraction (Batterman & Cole, 1964) and reveals the presence of point defects and their aggregates. It is interesting to see the shape of the DC. The DC is asymmetric with respect to the Bragg peak position. For a particular angular deviation ($\Delta\theta$) of glancing angle (θ) with respect to the Bragg peak position (taken as zero for the sake of convenience), the scattered intensity is much higher in the negative direction than in the positive direction. This feature clearly indicates that the crystal contains predominantly vacancy-type defects rather than interstitial defects, which may be a result of the oxygen vacancies as pointed out earlier. This can be well understood by the fact that, because of the presence of vacancy defects, the lattice around these defects undergoes tensile stress (Bhagavannarayana et al., 2008) and the lattice parameter d (interplanar spacing) increases. This results in more scattered
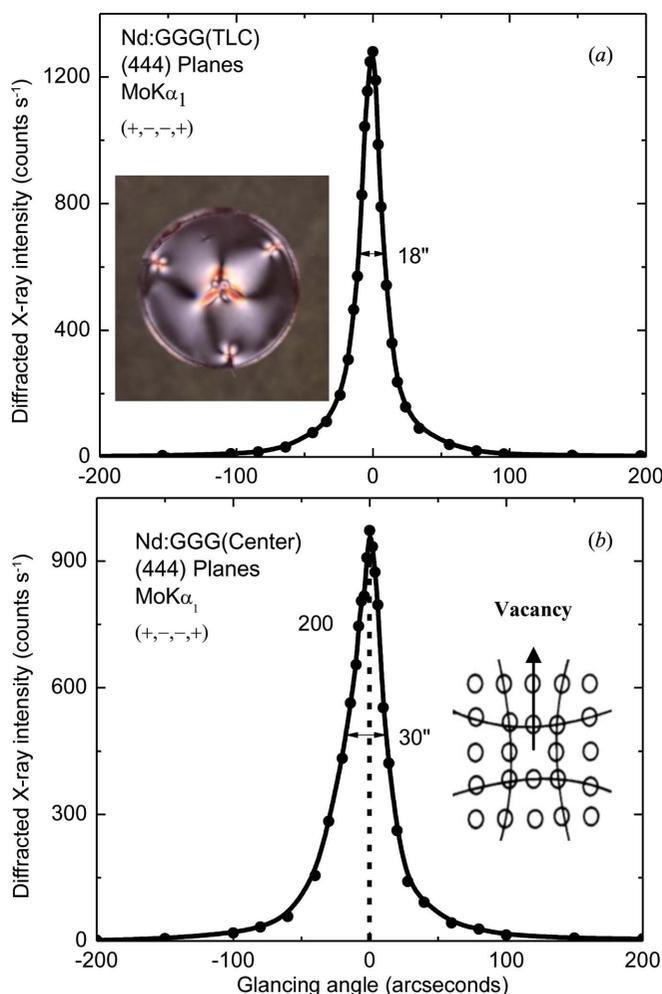
Figure 3
Diffraction curves recorded from (a) a clean portion and (b) the central regions of Nd:GGG grown with a steep convex interface. The inset in (b) shows a schematic of a vacancy defect.

(also known as diffuse X-ray scattering) intensity at slightly lower Bragg angles (θ_B) as d and $\sin\theta_B$ are inversely proportional to each other in the Bragg equation ($2d\sin\theta_B = n\lambda$, n and λ being the order of reflection and the wavelength, respectively, which are fixed). The inset in Fig. 3(b) shows a schematic illustrating how the lattice around the defect core undergoes tensile stress. It may be mentioned here that the

lattice spacing of the very limited number of atoms at the core of the defect may be lower, but the lattice spacing of the large number of surrounding planes around the defect core increases because of tensile stress. The converse explanation is true in the case of interstitial defects, which cause compressive stress in the lattice around the defect core, leading to a decrease of lattice spacing and in turn resulting in more
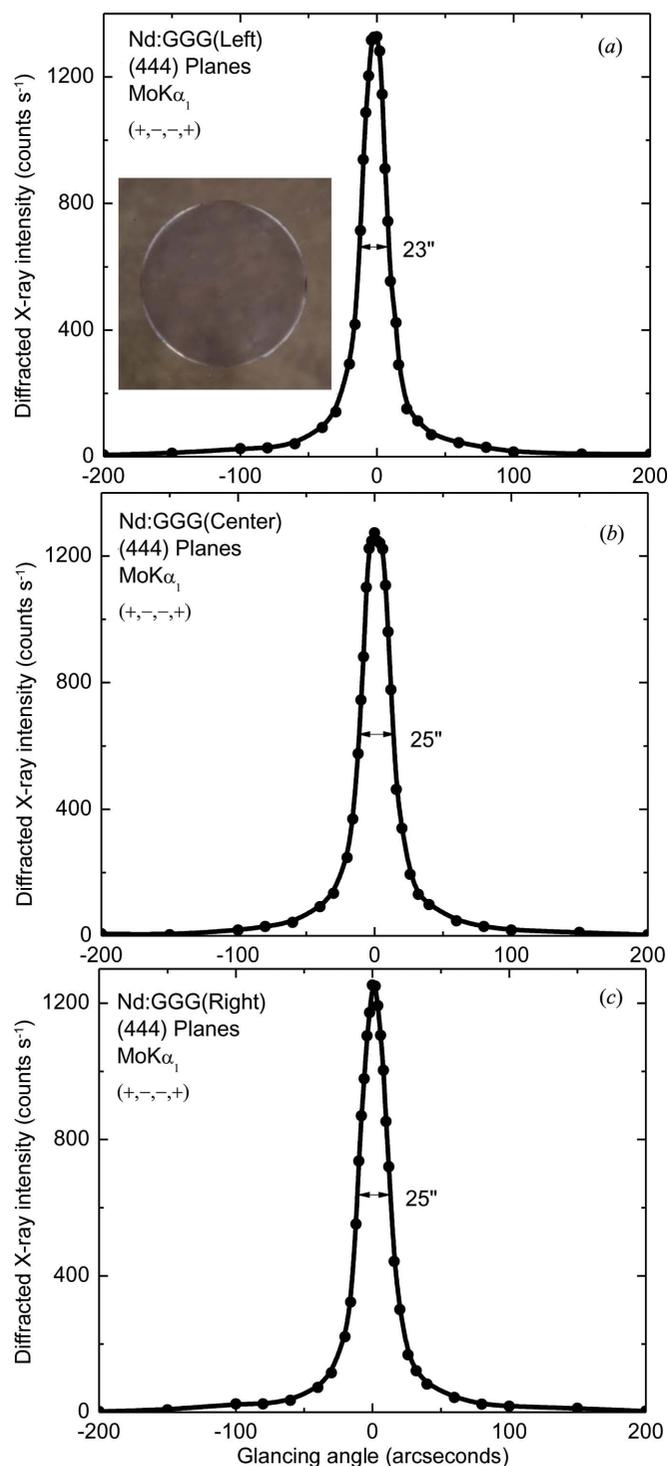
Figure 4
Diffraction curves recorded from (a) the left, (b) the central and (c) the right regions of Nd:GGG grown with a flat interface.
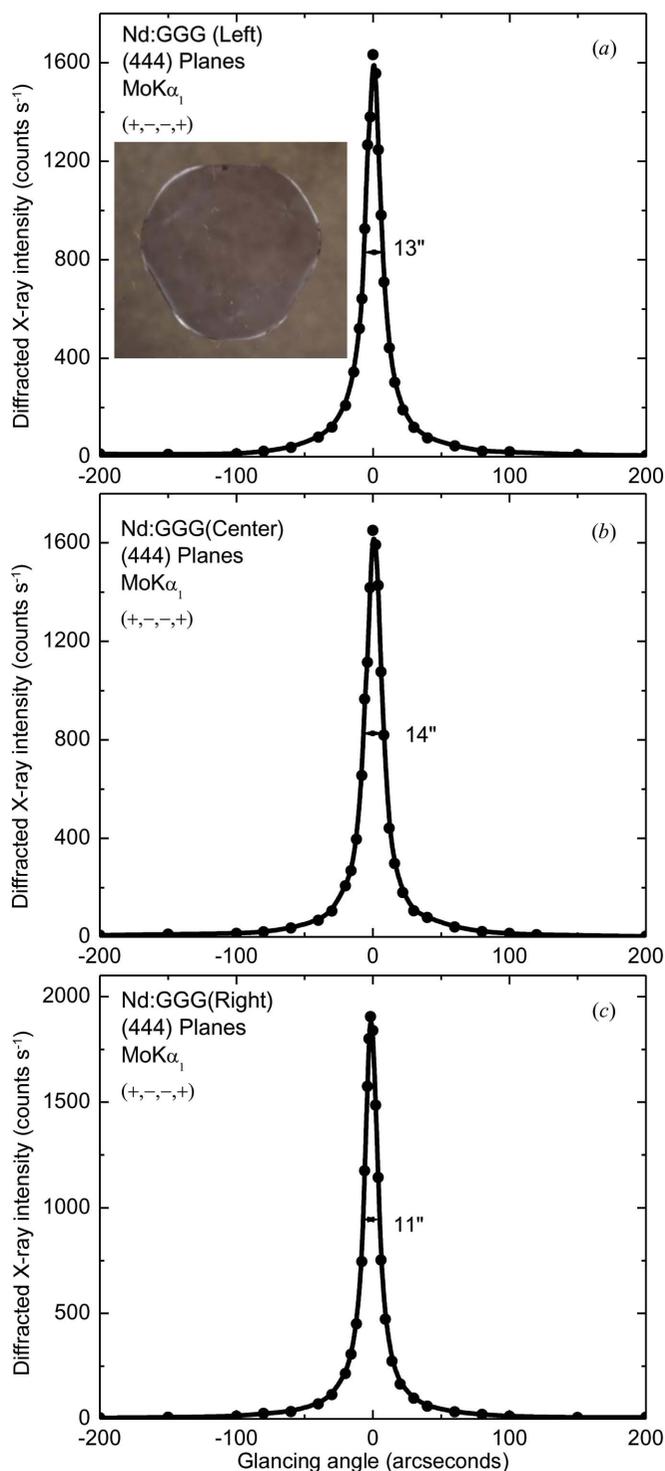
Figure 5
Diffraction curves recorded from (a) the left, (b) the central and (c) the right regions of Nd:GGG grown with a concave interface.

scattered intensity at the higher Bragg angles. It may be noted here that the variation in lattice parameter is confined to close to the defect core, which gives only the scattered intensity close to the Bragg peak. Long-range order could not be expected and hence a change in the lattice parameter is also not expected (Bhagavannarayana *et al.*, 2011). It may also be worth mentioning that the observed vacancy defects are more or less statistically distributed in the crystal. If these defects are not statistically distributed, but distributed here and there as macroscopic clusters, then the strain generated by such clusters is larger, leading to cracks and structural grain boundaries. These can be seen very clearly in HRXRD curves as additional peak(s), as observed in our recent study on urea-doped crystals in tristhioureazinc(II) sulfate at various levels of doping (Bhagavannarayana & Kushwaha, 2010). However, in the present experiments the diffraction curve does not contain any additional peaks, which indicates the absence of clustering of defects at the macroscopic level. The single diffraction peak with low FWHM indicates that the crystalline perfection is fairly good.

Fig. 4 shows the diffraction curves recorded from the left (*a*), central (*b*) and right (*c*) portions of a crystal [specimen (*b*) of Fig. 2, which is also shown in the inset] grown with a flat crystal/melt interface. The FWHMs of the three curves are almost the same, indicating that the crystal is equally perfect throughout. The sample under the polarizing microscope also showed uniform homogeneity. As the inhomogeneous central core is not present in crystals grown with a flat interface, a large slab can be fabricated out of such crystals, which can be used in the fabrication of high-power heat capacity solid-state lasers (HCSSLs).

Fig. 5 shows the diffraction curves recorded from the left (*a*), central (*b*) and right (*c*) portions of a crystal grown with a concave crystal/melt interface [specimen (*c*) of Fig. 2, which is also shown in the inset]. The FWHMs of the three curves are very narrow and have almost the same value, indicating that the crystal perfection is quite good and is equally perfect throughout. The sample under the polarizing microscope also showed uniform homogeneity. However, if the degree of concaveness is high and for crystal growth systems with a weight sensor for automatic diameter control, these conditions may lead to an increase in diameter of the crystal, which in turn will increase the degree of concaveness and may ultimately lead to termination of the crystal growth process. Though the crystal perfection is very good for such crystals grown with a concave interface, the crystal growth process is very unstable. Hence, by maintaining a high degree of concaveness at the interface, good crystals can be grown but with lesser thickness.

4. Conclusions

From a crystal perfection study using an optical polarizing microscope and HRXRD, it is clearly demonstrated that the crystal grown with a flat crystal/melt interface has uniform optical homogeneity as well as crystallographic perfection. As it has uniform properties, this kind of crystal can be used in the form of a slab as an active medium for high-power solid-state lasers such as HCSSLs. The crystal grown with a concave crystal/melt interface also has uniform optical homogeneity and crystallographic perfection. The crystalline perfection is shown to be best for crystals obtained with a concave interface; in this case the perfection is even better than that of the best portion of the crystal grown with a convex interface. Therefore, by maintaining a low degree of concaveness during growth by adjusting the crystal rotation, good quality crystals for slab fabrication may be grown. Crystals with a concave interface can be obtained by slightly increasing the crystal rotation rate from the initial condition of crystal rotation for a flat interface. However, owing to the lowering of the melt with the progress of crystal growth, without increasing the crystal rotation one can also obtain a concave interface. The present study reveals a novel correlation between optical inhomogeneity and crystalline perfection for a range of specimens with various shapes of crystal/liquid interface obtained through different seed rotation rates. We conclude that the best quality crystals are obtained when crystals are grown with a concave crystal/melt interface at an appropriate seed rotation rate in the Czochralski crystal growth method.

References

Batterman, B. W. & Cole, H. (1964). *Rev. Mod. Phys.* **36**, 681–717.
Bhagavannarayana, G. & Kushwaha, S. K. (2010). *J. Appl. Cryst.* **43**, 154–162.
Bhagavannarayana, G., Kushwaha, S. K., Shakir, Mohd. & Maurya, K. K. (2011). *J. Appl. Cryst.* **44**, 122–128.
Bhagavannarayana, G., Parthiban, S. & Meenakshisundaram, S. (2006). *J. Appl. Cryst.* **39**, 784–790.
Bhagavannarayana, G., Parthiban, S. & Meenakshisundaram, S. (2008). *Cryst. Growth Des.* **8**, 446–451.
Bhagavannarayana, G. & Zaumseil, P. (1997). *J. Appl. Phys.* **82**, 1172–1177.
Greber, J. F. (2002). *Gallium and Gallium Compounds* in *Ullmann's Encyclopedia of Industrial Chemistry*, doi:10.1002/14356007.a12_163. Weinheim: Wiley-VCH.
Janusz, Cz., Jelenski, W. & Niklas, A. (1982). *J. Cryst. Growth*, **57**, 593–596.
Keszei, B., Paitz, J., Vandlik, J. & Süveges, A. (2001). *J. Cryst. Growth*, **226**, 95–100.
Lal, K. & Bhagavannarayana, G. (1989). *J. Appl. Cryst.* **22**, 209–215.
Lupei, A., Stoicescu, C. & Lupei, V. (1997). *J. Cryst. Growth*, **177**, 207–210.
Senthil Kumar, K., Moorthy Babu, S. & Bhagavannarayana, G. (2011). *J. Appl. Cryst.* **44**, 313–318.
Stacy, W. T., Metselaar, R., Larsen, P. K., Bril, A. & Pistorius, J. A. (1974). *Appl. Phys. Lett.* **24**, 254–256.
Zimik, K., Chauhan, R. R., Kumar, R., Murari, K., Malhan, N. & Thakur, H. V. (2013). *J. Cryst. Growth*, **363**, 76–79.